RSC Advances

PAPER

View Article Online
View Journal | View Issue



Cite this: *RSC Adv.*, 2018, **8**, 19157

# 3D zinc@carbon fiber composite framework anode for aqueous Zn–$MnO_2$ batteries†

Wei Dong, [ab] Ji-Lei Shi, [ab] Tai-Shan Wang, [ab] Ya-Xia Yin, [ab] Chun-Ru Wang *[ab] and Yu-Guo Guo *[ab]

Received 15th April 2018
Accepted 13th May 2018

DOI: 10.1039/c8ra03226b

rsc.li/rsc-advances

Rechargeable aqueous batteries are one of the most promising large-scale energy storage devices because of their environment-friendly properties and high safety advantages without using flammable and poisonous organic liquid electrolyte. In addition, rechargeable Zn–$MnO_2$ batteries have great potential due to their low-cost resources as well as high energy density. However, dendritic growth of the zinc anode hinders the exertion of cycling stability and rate capacity in an aqueous Zn–$MnO_2$ battery system. Here we use an electrochemical deposition method to *in situ* form a three-dimensional (3D) zinc anode on carbon fibers (CFs). This 3D Zn@CFs framework has lower charge transfer resistance with larger electroactive areas. Batteries based on the 3D zinc framework anode and α-$MnO_2$ nanowire cathode present enhanced rate capacity and long cycling stability, which is promising for utilization in other zinc anode based aqueous batteries as an effective way to solve dendrite formation.



## 1. Introduction

Lithium ion batteries have been widely used as portable energy storage devices with high energy density and long cycle stability.[1–3] However, the growing concerns about high costs, poor safety and earth-limited element resources of Li-ion batteries have revived Li-free aqueous batteries, especially in large-scale energy storage systems.[4–8] Among them, battery reactions based on reversible insertion of $Na^+$, $K^+$, $Mg^{2+}$ and $Zn^{2+}$ and hybrid ions in mild aqueous electrolyte have been considered as promising alternatives, because of their high safety, material abundance, non-flammability and environmentally friendly properties.[9,10] In an aqueous system, the narrow voltage window of water (1.23 V *vs.* SHE) restricts the options of electrode material, especially for the anode materials. Among these, rechargeable aqueous Zn/$MnO_2$ batteries are considered as one of the most attractive alternatives which have been extensively studied for several years.[11–14]

Zn and Mn elements are all earth abundant with affordable prices and can be largely utilized in an aqueous energy storage system. Zn metal anode has an appropriate voltage potential (−0.76 V *vs.* SHE) and a high theoretical capacity (825 mA h $g^{-1}$).[15] In the meantime, $MnO_2$ with α-, β- or amorphous phases is easily fabricated and the whole system is environment friendly.[16,17] However, poor cycle life and the growth of Zn dendrites[18–20] hinder the development and commercialization of rechargeable Zn–$MnO_2$ batteries. Primary Zn dendrites can puncture the diaphragm, causing short circuits. Lots of approaches have been proposed to optimize these problems such as adding additives in the electrolyte to modify the deposition behavior,[21,22] coating a new protective layer on the surface of Zn metal[23,24] or using Zn-alloy[25–27] to improve conductivity and anti-corrosion property. Unfortunately, most of the improvements are either expensive or hard to maintain a long lifespan during cell cycling.

Here, a composited Zn anode is introduced by constant voltage (−1.4 V *vs.* SHE) electrodepositing zinc on three-dimensional (3D) carbon fibers (CFs) to solve dendrite growth

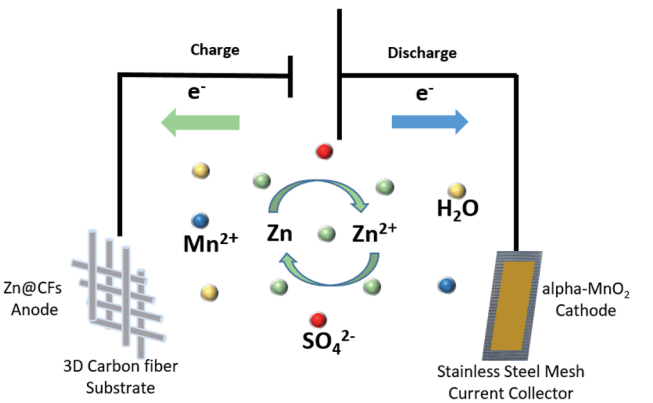


Fig. 1 Schematic illustration of Zn@CFs|2.0 mol $l^{-1}$ $ZnSO_4$, 0.1 mol $l^{-1}$ $MnSO_4$|α-$MnO_2$ aqueous battery.

[a]CAS Key Laboratory of Molecular Nanostructure and Nanotechnology, CAS Research/Education Center for Excellence in Molecular Sciences, Institute of Chemistry, Chinese Academy of Sciences (CAS), Beijing 100190, P. R. China. E-mail: ygguo@iccas.ac.cn

[b]University of Chinese Academy of Sciences, Beijing 100049, P. R. China

† Electronic supplementary information (ESI) available. See DOI: 10.1039/c8ra03226b

issues in a Zn–$MnO_2$ battery system during cycling. The Zn@CFs core–shell structure provides zinc anode with larger electrochemical reaction area[28] and can withstand the inside strain and stress during Zn plating or stripping process. By combining this 3D dendrite-free Zn anode with the α-$MnO_2$ nanofiber cathode, an aqueous full cell (Fig. 1) with excellent electrochemical performance is fabricated with ultra-stable cycling performance and no dendrite growth was found even

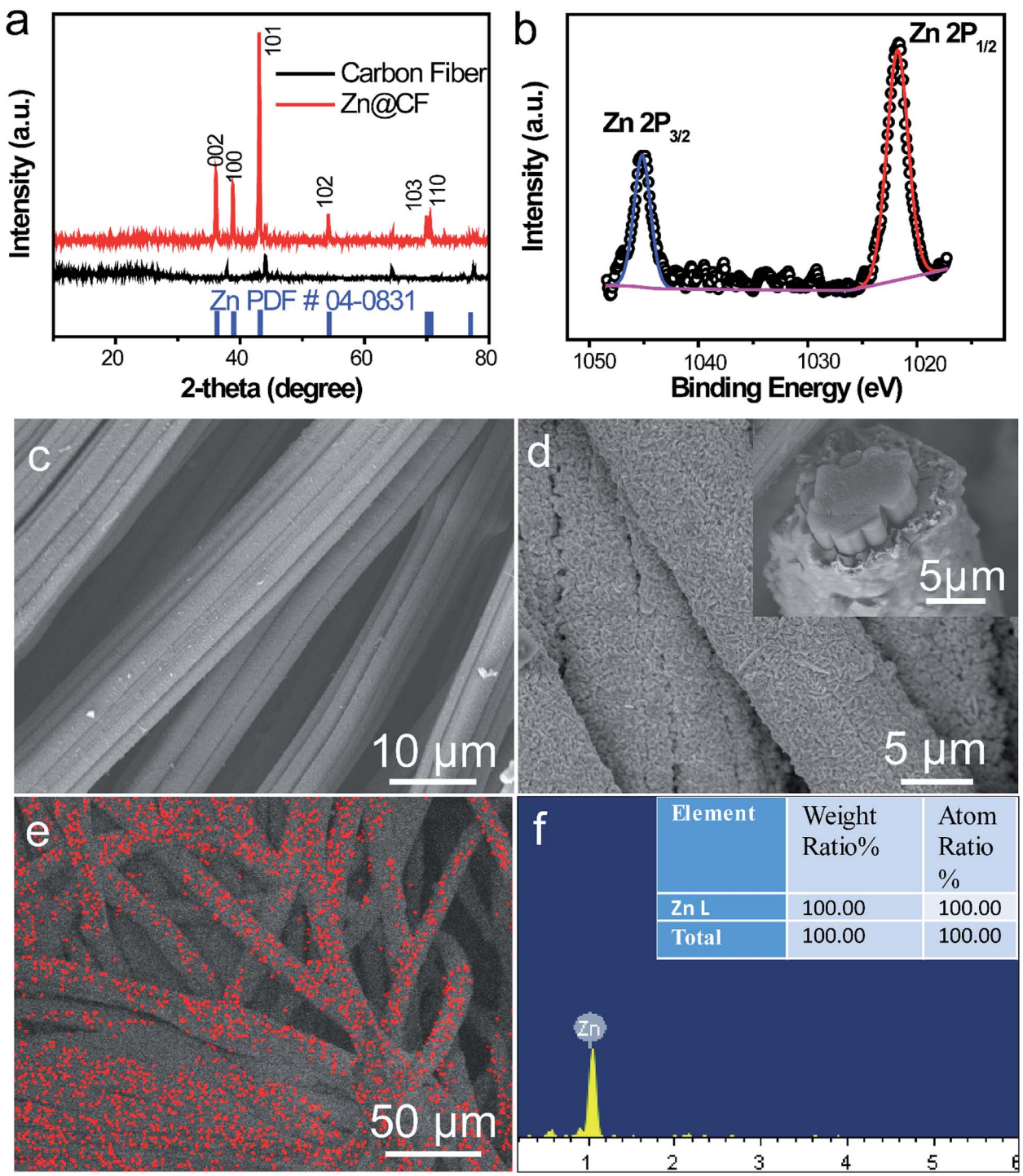


Fig. 2 Characterizations of Zn@CFs composite anode. (a) XRD patterns of Zn@CFs and pristine carbon fiber substrate. (b) XPS spectrum of the as-prepared Zn@CFs anode. (c and d) SEM images of pristine carbon fiber substrate and Zn@CFs anode, the image inside (d) is a cross-view of Zn@CFs anode. (e and f) Mapping image and EDS test of the as-prepared Zn@CFs anode, Zn element was marked in red (e).

after 140 cycles at a cycling current density of 308 mA $cm^{-2}$. This study also provides insights to reconcile the demands for both dendrite-free structure modification engineering and good cycling stability faced in the practical use of the aqueous rechargeable Zn/$MnO_2$ energy storage system.[29–33]

## 2. Experimental

### 2.1 Material synthesis

Preparation of the 3D flexible Zn@CFs anode: as schematically shown in Fig. s1,† the electrodeposition process was carried out in a three-electrode glass cell consists of a hydrophilic carbon clothes (350 μm thick, Shanghai Hesen, 99%) as working electrode, a Pt foil (Alfa, 99%) as counter electrode, a SCE as the reference electrode.[34] The electrodeposition voltage was under −1.4 V (*vs.* SCE) for 0.5 h. The α-$MnO_2$ nanofibers cathode was synthesized through a hydrothermal method.[35] Briefly, 0.003 M $MnSO_4 \cdot H_2O$, 2 ml 0.5 M $H_2SO_4$ and 20 ml 0.1 M $KMnO_4$ were in order added to 90 ml deionized water and then transferred to a Teflon-lined autoclave and heated at 120 °C for 12 h. The mass load of the cathode material was about 2 mg $cm^{-2}$ and the deposition amount of Zn was about 7.85 mA h $cm^{-2}$ (see ESI, Fig. s2 and s3†). Then, the as-prepared electrodes and the Whatman glass fiber separator were used to fabricate a Zn–$MnO_2$ battery.

### 2.2 Materials characterizations

The scanning electron microscopy images and corresponding Energy Dispersive Spectrometer (EDS) and mapping images were obtained by JEOL 6701F. X-ray photoelectron spectroscopy (XPS) and X-ray diffraction (XRD) patterns were recorded by the ESCALab 250Xi spectrometer and Rigaku D/max-2500 diffractometer, respectively. The High Resolution Transmission Electron Microscopy (HRTEM) images were examined on the JEM 2100F at an accelerating voltage of 200 kV. The Brunauer–Emmett–Teller (BET) surface area was measured by nitrogen adsorption–desorption using a Quantachrome Autosorb-IQ MP.

### 2.3 Electrochemical characterization

Zn@CFs plating or stripping test was conducted by assembling a symmetric battery based on Zn foil as the counter/reference electrode, Zn@CFs as the working electrode. As a contrast experiment, the same amount of Zn (7.85 mA h $cm^{-2}$) was deposited on a 2D stainless steel current collector as work electrode and then assembled in the same way to testify the superior cycling stability of this 3D composite structure, this control sample was named as Zn@SS. The cycling stability was measured at a current of 1 mA $cm^{-2}$ for 1 h between each plating or stripping stage. CR2032-type coin full cell was assembled with Zn@CFs anode, glass fiber separator and α-$MnO_2$ nanowire cathode. The electrolyte used in this work was a mixture of 2 M $ZnSO_4$ and 0.1 M $MnSO_4$ in $H_2O$ solution at a pH of 5–6. The capacity evaluation of the full cell was based on the load of cathode mass. Active materials (α-$MnO_2$ nanowire) : conductive additive (Super P) : polytetrafluoroethylene (PTFE) were mixed in a rate of 7 : 2 : 1 to form a slurry with ethanol solution and rolled onto the stainless-steel current collector to make a cathode electrode. Cyclic voltammetry (CV) was performed by a Princeton electrochemical work station (ParSTAT MC). Galvanostatic tests were measured by using LAND cycler (Kingnuo Electronic Co., China) at room temperature.

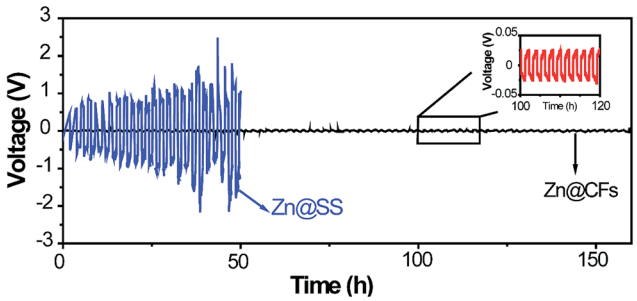


Fig. 4 Voltage profile of Zn@CFs|Zn symmetric cell (black line) and Zn@SS|Zn symmetric cell (blue line) in plating/stripping process.

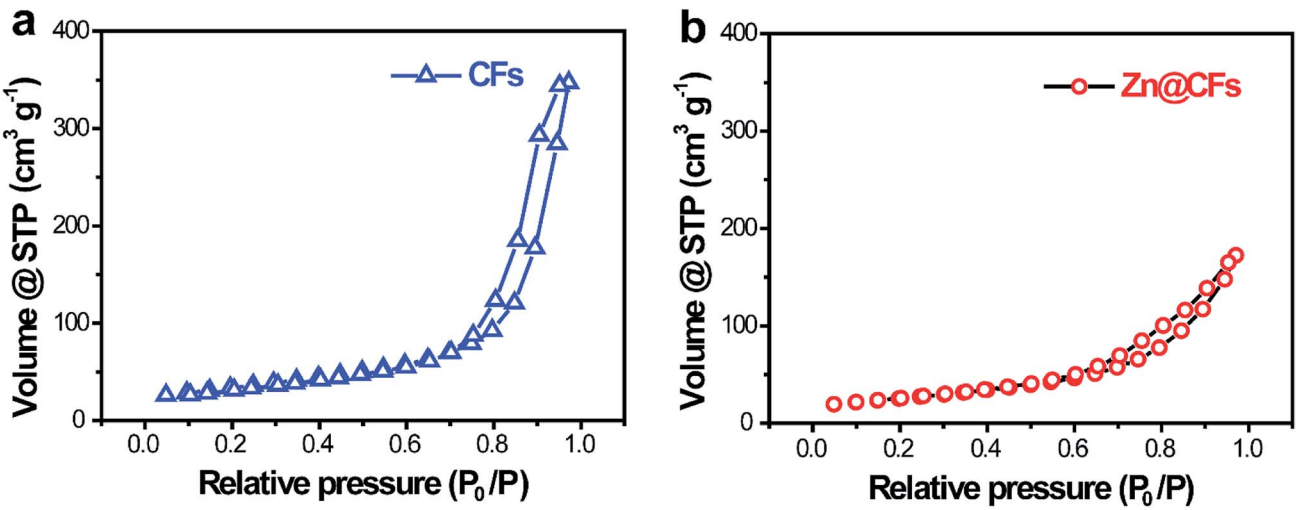


Fig. 3 $N_2$ adsorption/desorption isotherms of (a) pristine carbon fiber substrate and (b) the as-prepared Zn@CFs composite anode.

# 3. Results and discussion

## 3.1 Zn@CFs composite anode characterization

To characterize the structure of the obtained electrodes, XRD tests were performed. The patterns (Fig. 2a) of the as-prepared Zn@CFs showed that all the main peaks match with metal zinc's base peak (JCPSD: 04-0831). After deposition, carbon fibers' peaks were weakened or disappeared which indicate that a uniform deposition layer on the surface of 3D carbon fiber framework was achieved. Also, XPS spectrum (Fig. 2b) shows that two peaks at 1021.75 eV (Zn $2P_{1/2}$) and 1044.7 eV (Zn $2P_{3/2}$) were detected which were attributed to the signal of pure Zn metal. The morphology changes before and after deposition process were observed by SEM. Before deposition, the surface of carbon fiber was smooth and flat (Fig. 2c), after constant voltage deposition, a uniform Zn metal layer with a rough surface (Fig. 2d) was *in situ* coated on the carbon fibers. The thickness of compactly deposited Zn metal layer was about 2 μm (Fig. 2d, inner image). The mapping image (Fig. 2e) of deposited zinc was marked in red which showed that a large-scale uniform deposition of Zn on the carbon-fiber substrate. The EDS result (Fig. 2f) was well-indexed with XRD and XPS results that the one and only peak of Zn (100%) was detected on the surface of Zn@CFs.

The BET isotherms of $N_2$ adsorption and desorption were conducted at 77 K before and after Zn deposition (Fig. 3a and b). Compared with one dimensional commercialized Zn plate with a negligible active area ($1.12 \times 10^{-3}$ $m^2$ $g^{-1}$), the determined specific surface area of pristine 3D carbon fiber framework was 121.2 $m^2$ $g^{-1}$ which provide dramatically enlarged electroactive area that can lower charge transfer resistance. After deposition, the determined specific surface area of as-prepared Zn@CFs was slightly decreased to 91.3 $m^2$ $g^{-1}$ but still much higher than commercialized Zn plate. The unique composite anode design combined high electroactive area with high conductive skeleton, which lay the foundation for an effective electrochemical performance.

Zn@CFs plating or stripping test was conducted by assembling a symmetric battery based on Zn foil as the counter/reference electrode, Zn@CFs as working electrode. As a contrast experiment, the same amount of Zn (7.85 mA h $cm^{-2}$) was deposited on a 2D stainless steel current collector (Zn@SS) as work electrode and then assemble in the same way to testify the superior cycling stability of this 3D composite structure. The cycling stability was measured at a current of 1 mA $cm^{-2}$ for 1 h between each plating or stripping stage. The galvanostatic plating/stripping of Zn@CFs anode (Fig. 4) showed that an

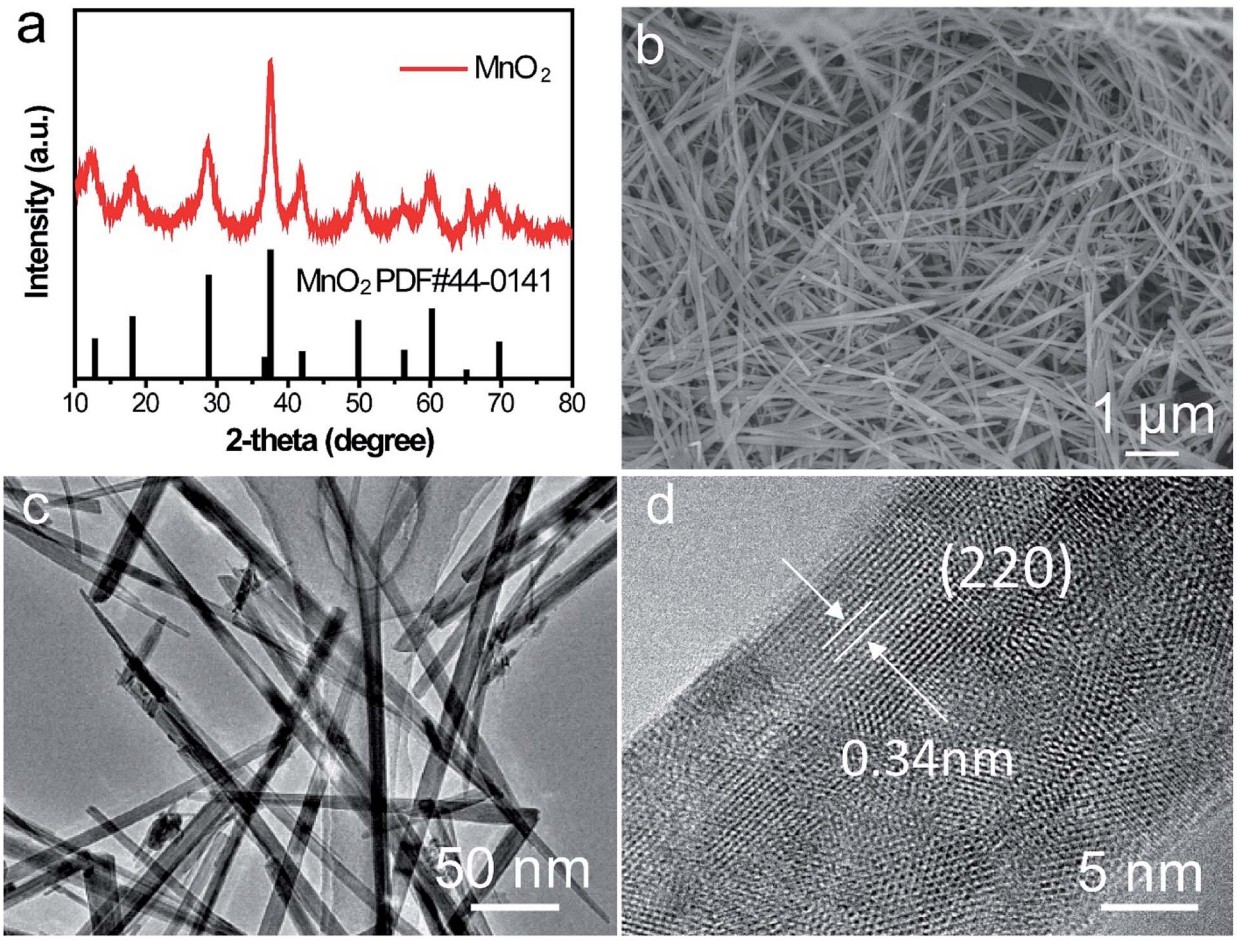


Fig. 5 Characterizations of α-$MnO_2$ nanowire cathode. (a) XRD patterns of the as-prepared α-$MnO_2$, (b) SEM image, (c) TEM image and (d) magnified TEM image.

 

ultra-low potential fluctuation (less than 30 mV) exhibit which prove the superior electrochemical stability of this novel designed 3D framework. However, without the use 3D conductive framework, a symmetric battery based on 2D stainless steel substrate show huge unsteadiness and drastic fluctuations during plating/stripping process.

### 3.2 α-$MnO_2$ nanowire cathode characterization

The crystalline phase of as-prepared α-$MnO_2$ nanowire was shown in (Fig. 5a) which fully complexed with the base peak α-$MnO_2$ (JCPDS: 44-0141). The length of the α-$MnO_2$ nanowire was a few micrometres which was observed by SEM (Fig. 5b). TEM image of α-$MnO_2$ nanofibers was shown in Fig. 5c with a homogeneous one-dimensional (1D) nanofibre structure and a diameter of 20 nm, lattice fringes along the (220) planes was shown in Fig. 5d, which revealed that the as-prepared α-$MnO_2$ was highly crystalline.[36]

### 3.3 Zn@CFs anode|α-$MnO_2$ cathode full cell characterization

To further ascertain the superiority in liberating the electrochemical property and cycling stability of this Zn@CFs anode, a full aqueous battery with α-$MnO_2$ nanofiber cathode in a mild aqueous electrolyte was assembled. The capacity evaluation of the full cell was based on the load of cathode mass and the theoretical capacity of α-$MnO_2$ was 308 mA h $g^{-1}$ (1C). The operational voltage window of the system was evaluated by voltammetry at 0.5 mV $s^{-1}$ in Fig. 6a, which two pairs of redox peaks are consistent with the two plateaux in the charge/discharge curves in Fig. 6b. Decent capacities of 275.2, 248.2, 182.0 mA h $g^{-1}$ were delivered for the full cells at different current rates of 1/3C, 1C and 2C, respectively. Even at a high rate of 5C, a discharge capacity of 119.3 mA h $g^{-1}$ was obtained, which showed an excellent rate capability of this system. For the long-term cycling performance (Fig. 6c) at a rate of 1C, the initial discharge capacity was 239.4 mA h $g^{-1}$ and after 140 cycles, the corresponding capacity retention was 86.8%. This high-rate performance could be ascribed to the stabilization and excellent kinetics 3D anode framework design with lower charge transfer resistance and larger electroactive areas. The comparison of the electrical performance of the as-obtained Zn@CFs/$MnO_2$ aqueous battery with previous reported $Zn^{2+}$ ion aqueous battery systems was listed on Table S1.†

The morphology changes of a commercialized zinc plate anode before and after cycling test were shown in (Fig. s4a and b†). During the cycling process, Zn dendrite was formed because of

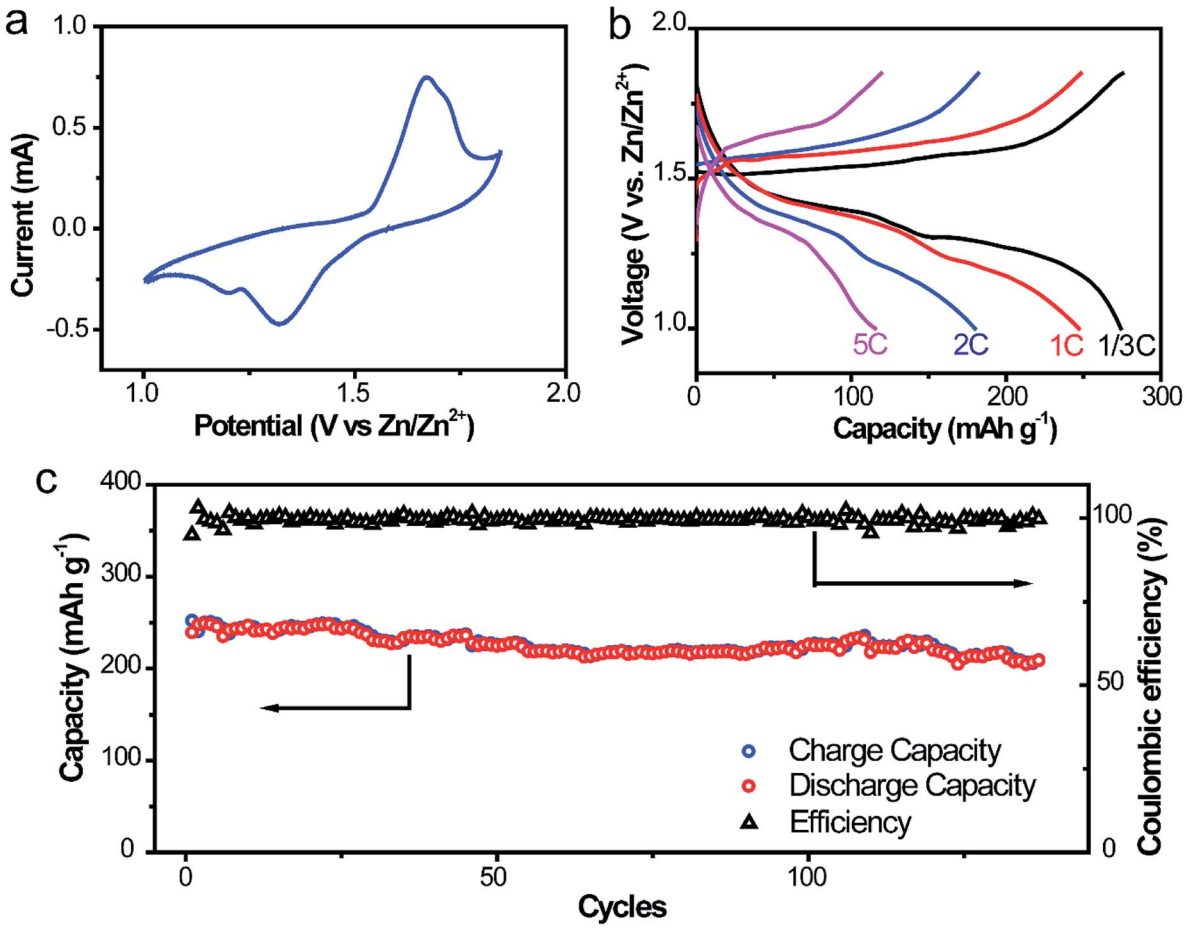


Fig. 6 (a) CV scanning profile at 0.5 mV $s^{-1}$ (b) galvanostatic discharging/charging profiles at 1/3, 1, 2, 5C rate, respectively. (c) Cycling performances of Zn@CFs|α-$MnO_2$ full cell at 1C rate.

uneven deposition and increasing irreversible side-reactions during the charging–discharging processes, which led to battery failures. This result confirmed that Zn@CFs anode reconciled the stability with excellent electrical performance. The structure stability of this 3D framework electrode was tested by comparing the morphology Zn@CFs before and after cycling test. Through SEM images (Fig. s4c and d†), it can be seen that even after 140 cycles at 1C, the compact 3D structure remained and Zn still preferentially deposited on the surface of CFs without any structure collapse or dendrite growth.

## 4. Conclusion

In conclusion, we have proposed a novel three-dimensional structure of zinc anode through constant voltage electrodeposition method on a conductive carbon skeleton, which offers lower charge transfer resistance and larger electroactive areas in suppressing zinc dendritic growth. Full batteries based on this 3D Zn@CFs anode and $\alpha$-$MnO_2$ exhibit an excellent rate capability and a long-term cycling stability at high rates. This design strategy will inspire a deep comprehension of integral structure of Zn-based aqueous battery for other aqueous large-scale energy storage systems.

## Conflicts of interest

The authors declare that they have no conflict of interest.

## Acknowledgements

This wok was supported by the Basic Science Center Project of National Natural Science Foundation of China under grant No. 51788104, the National Key R&D Program of China (Grant No. 2016YFA0202500), the National Natural Science Foundation of China (21773264, 51672281) and the "Transformational Technologies for Clean Energy and Demonstration", Strategic Priority Research Program of the Chinese Academy of Sciences (Grant No. XDA 21070300).

## Notes and references

1 J. B. Goodenough and Y. Kim, *Chem. Mater.*, 2010, **22**, 587–603.
2 D. Lin, Y. Liu and Y. Cui, *Nat. Nanotechnol.*, 2017, **12**, 194–206.
3 J. M. Tarascon and M. Armand, *Nature*, 2001, **414**, 359–367.
4 R. K. Guduru and J. C. Icaza, *Nanomaterials*, 2016, **6**, 3.
5 J. Liu, J.-G. Zhang, Z. Yang, J. P. Lemmon, C. Imhoff, G. L. Graff, L. Li, J. Hu, C. Wang, J. Xiao, G. Xia, V. V. Viswanathan, S. Baskaran, V. Sprenkle, X. Li, Y. Shao and B. Schwenzer, *Adv. Funct. Mater.*, 2013, **23**, 929–946.
6 W. He, X. Luo, D. Evans, J. Busby, S. Garvey, D. Parkes and J. Wang, *Appl. Energy*, 2017, **208**, 745–757.
7 S. Kapila, A. O. Oni and A. Kumar, *Energy*, 2017, **140**, 656–672.
8 D. Laslett, C. Carter, C. Creagh and P. Jennings, *Renewable Energy*, 2017, **113**, 713–731.
9 M. Yan, P. He, Y. Chen, S. Wang, Q. Wei, K. Zhao, X. Xu, Q. An, Y. Shuang, Y. Shao, K. T. Mueller, L. Mai, J. Liu and J. Yang, *Adv. Mater.*, 2018, **30**, 1703725.
10 N. Zhang, F. Cheng, J. Liu, L. Wang, X. Long, X. Liu, F. Li and J. Chen, *Nat. Commun.*, 2017, **8**, 405.
11 C. Xu, B. Li, H. Du and F. Kang, *Angew. Chem., Int. Ed.*, 2012, **51**, 933–935.
12 H. Li, C. Xu, C. Han, Y. Chen, C. Wei, B. Li and F. Kang, *J. Electrochem. Soc.*, 2015, **162**, A1439–A1444.
13 C. Han, Y.-B. He, M. Liu, B. Li, Q.-H. Yang, C.-P. Wong and F. Kang, *J. Mater. Chem. A*, 2017, **5**, 6368–6381.
14 H. Li, C. Han, Y. Huang, Y. Huang, M. Zhu, Z. Pei, Q. Xue, Z. Wang, Z. Liu, Z. Tang, Y. Wang, F. Kang, B. Li and C. Zhi, *Energy Environ. Sci.*, 2018, **11**, 941–951.
15 H. Kim, G. Jeong, Y.-U. Kim, J.-H. Kim, C.-M. Park and H.-J. Sohn, *Chem. Soc. Rev.*, 2013, **42**, 9011–9034.
16 C. Xu, H. Du, B. Li, F. Kang and Y. Zeng, *Electrochem. Solid-State Lett.*, 2009, **12**, A61–A65.
17 M. H. Alfaruqi, V. Mathew, J. Gim, S. Kim, J. Song, J. P. Baboo, S. H. Choi and J. Kim, *Chem. Mater.*, 2015, **27**, 3609–3620.
18 J. F. Parker, E. S. Nelson, M. D. Wattendorf, C. N. Chervin, J. W. Long and D. R. Rolison, *ACS Appl. Mater. Interfaces*, 2014, **6**, 19471–19476.
19 Y. W. Shen and K. Kordesch, *J. Power Sources*, 2000, **87**, 162–166.
20 Y. Ito, M. Nyce, R. Plivelich, M. Klein, D. Steingart and S. Banerjee, *J. Power Sources*, 2011, **196**, 2340–2345.
21 C. W. Lee, K. Sathiyanarayanan, S. W. Eom, H. S. Kim and M. S. Yun, *J. Power Sources*, 2006, **160**, 161–164.
22 M. Azhagurajan, A. Nakata, H. Arai, Z. Ogumi, T. Kajita, T. Itoh and K. Itaya, *J. Electrochem. Soc.*, 2017, **164**, A2407–A2417.
23 M. A. Gonzalez, R. Trocoli, I. Pavlovic, C. Barriga and F. La Mantia, *Electrochem. Commun.*, 2016, **68**, 1–4.
24 T. K. A. Hoang, D. T. Nam Long, J. H. Cho, J. Y. J. Su, C. Lee, C. Lu and P. Chen, *Chemsuschem*, 2017, **10**, 2816–2822.
25 A. Varzi, L. Mattarozzi, S. Cattarin, P. Guerriero and S. Passerini, *Adv. Energy Mater.*, 2018, **8**, 1701706.
26 S. Shuai, E. Guo, M. Wang, M. D. Callaghan, T. Jing, Q. Zheng and P. D. Lee, *Metall. Mater. Trans. A*, 2016, **47**, 4368–4373.
27 M. Y. Wang, Y. J. Xu, T. Jing, G. Y. Peng, Y. N. Fu and N. Chawla, *Scr. Mater.*, 2012, **67**, 629–632.
28 L.-P. Wang, N.-W. Li, T.-S. Wang, Y.-X. Yin, Y.-G. Guo and C.-R. Wang, *Electrochim. Acta*, 2017, **244**, 172–177.
29 Y. Lu, J. B. Goodenough and Y. Kim, *J. Am. Chem. Soc.*, 2011, **133**, 5756–5759.
30 J. Abad, F. Santos, J. P. Tafur, A. Urbina, E. Roman, J. F. Gonzalez-Martinez, J. Rubio-Zuazo, G. R. Castro and A. J. Fernandez Romero, *J. Power Sources*, 2017, **363**, 199–208.
31 W. Qiu, Y. Li, A. You, Z. Zhang, G. Li, X. Lu and Y. Tong, *J. Mater. Chem. A*, 2017, **5**, 14838–14846.
32 W. Sun, F. Wang, S. Hou, C. Yang, X. Fan, Z. Ma, T. Gao, F. Han, R. Hu, M. Zhu and C. Wang, *J. Am. Chem. Soc.*, 2017, **139**, 9775–9778.
33 Y. Zeng, X. Zhang, Y. Meng, M. Yu, J. Yi, Y. Wu, X. Lu and Y. Tong, *Adv. Mater.*, 2017, **29**, 1700274.

 

34 X. Wang, F. Wang, L. Wang, M. Li, Y. Wang, B. Chen, Y. Zhu, L. Fu, L. Zha, L. Zhang, Y. Wu and W. Huang, *Adv. Mater.*, 2016, **28**, 4904–4911.

35 H. Pan, Y. Shao, P. Yan, Y. Cheng, K. S. Han, Z. Nie, C. Wang, J. Yang, X. Li, P. Bhattacharya, K. T. Mueller and J. Liu, *Nat. Energy*, 2016, **1**, 16309.

36 K. Zhong, B. Zhang, S. Luo, W. Wen, H. Li, X. Huang and L. Chen, *J. Power Sources*, 2011, **196**, 6802–6808.